Overview of the tunable beamlines for protein crystallography at the EMBL Hamburg Outstation; an analysis of current and future usage and developments

Ehmke Pohl,* Ana González,[1] Christoph Hermes and Roelof G. van Silfhout[2]*

European Molecular Biology Laboratory, Hamburg Outstation, Notkestr. 85, 22603 Hamburg, Germany. E-mail: ehmke@embl-hamburg.de; r.silfhout@umist.ac.uk

The EMBL Hamburg Outstation currently operates two tunable protein crystallography beamlines suitable for single and multiple anomalous diffraction (SAD/MAD) experiments. The first beamline, designated X31, is located on a bending magnet of the DORIS III storage ring whereas the second beamline, BW7A, is positioned at a multipole wiggler at the same storage ring. X31 is equipped with an energy stabilization device to ensure constant wavelength during longer data-collection periods. The in-house built crystallographic end-station is now equipped with a Mar345 imaging-plate scanner as a detector. The wiggler beamline BW7A features a novel sagitally focusing monochromator. The end-station used here has also been developed and built in-house. The beamline is currently operated with a Mar165 CCD detector. In this paper the hardware and software developments of the last years will be summarized and the outlook for substantial upgrades will be given. The future plans include the design and construction of a third tunable beamline, designated X12, for protein crystallography. The development of automated beamlines for protein crystallography is of particular importance with respect to structural genomics initiatives. The analysis of the projects of the last years shows the wide range of anomalous scatterer used on the tunable beamlines thus demonstrating the need of a wide range of accessible energies and fast and reliable energy changes.

Keywords: beamlines; anomalous diffraction; SAD; MAD; protein crystallography.

1. Introduction

Over the last years the multiple anomalous diffraction (MAD) method has emerged as a powerful tool for the solution of the phase problem in protein crystallography. A number of technical developments have contributed to the recent progress: (i) the development of tunable synchrotron beamlines (reviewed by Helliwell, 1992); (ii) the introduction of image-plate (Amemiya, 1997) and more recently charged-coupled-device (CCD) based detectors (Tate *et al*., 1995; Phillips *et al*., 2000); (iii) advances in the incorporation of selenomethionine into recombinant proteins (Doublie, 1997); (iv) cryo-cooling techniques that minimize radiation damage (Hope, 1988; Rodgers, 1997; Garman & Schneider, 1997; Garman, 1999); and (v) programs for automated structure solution and refinement such as *SOLVE* (Terwilliger & Berendzen, 1999), *CNS* (Brünger *et al*., 1998; Grosse-Kunstleve & Brünger, 1999), *SHARP* (La Fortelle & Bricogne, 1997) and *ARP*/*wARP* (Perrakis, Morris & Lamzin, 1999). In a MAD experiment the anomalous scattering from heavy atoms is used to determine the phases for a set of structure factors. Typically, diffraction data recorded at three different wavelengths near the absorption edge of the particular heavy atom are sufficient for determining the positions of the heavy atoms and subsequently the phases. The underlying mathematical and methodical aspects have already been covered in a number of excellent review articles and are beyond the scope of this article (see, for example, Hendrickson, 1990, 1999; Smith, 1991; Fourme *et al*., 1999; Walsh *et al*., 1999; Cassetta *et al*., 1999). Anomalous diffraction data collected at a single wavelength alone can only resolve the phase ambiguity using additional constraints. A number of recent studies have shown the potential of density modification techniques such as non-crystallographic symmetry averaging and solvent flattening to derive interpretable electron density from SAD experiments. Revisiting work by Hendrickson & Teeter (1981), it has been shown that the anomalous contribution from sulphur alone at the Cu K_α energy can be sufficient for structure solution (Dauter *et al*., 1999). Furthermore, SAD data collected at the maximum f'' wavelength (usually referred to as peak wavelength) of bromine (Dauter & Dauter, 1999) and selenium (Rice *et al*., 2000) has been used successfully for structure determination.

At the EMBL Hamburg Outstation two tunable beamlines suitable for SAD/MAD data collection have been designed and are now fully operational. The first beamline, X31, is located on a bending magnet of the DORIS III storage ring. This beamline has been in operation for MAD experiments since 1995. During that time the equipment has undergone various upgrades and improvements. The second beamline, designated BW7A, is placed on a 56-pole wiggler at DORIS III. Beamline BW7A has been used for macromolecular structure determination since 1997. A novel focusing monochromator was installed at this beamline in 1998 and after a short commissioning period the beamline was returned to the structural biology community in spring 1999. In this article, we discuss recent developments of these two EMBL synchrotron beamlines. In addition, we will show examples of novel crystal structures solved using data collected at the EMBL beamlines and give an outline of our future plans for the development of existing and new facilities at the EMBL Hamburg Outstation.

2. Overview of X31

Beamline X31 is located on a bending magnet of the DORIS III storage ring. The total fan of radiation is shared by four experimental stations leaving about 3 mrad for beamline X31. The positron beam size at the tangent point is approximately 2×0.5 mm^2 FWHM, with horizontal and vertical divergences of 0.4 mrad and 0.02 mrad, respectively. At 4.5 GeV positron energy, which is the standard operation mode for dedicated synchrotron radiation use, the critical energy of the emitted X-ray spectrum is around 16 keV (0.773 Å), given by the dipole magnet's bending radius of 12 m and the positron energy.

Since the basic set-up of beamline X31 has been described previously by Wilson (1989), we will focus here on the key components only. All optical elements of the beamline are operated under high-vacuum conditions and separated from the storage ring and the experimental hutch by beryllium windows. A set of vertical slits positioned about 15 m downstream of the source point constitutes the first optical element. This slit system reduces the heat load on the monochromator crystal, collimates and reduces the energy bandpass of the beam. The next optical element is a Si(111) channel-cut monochromator, which is mounted on a water-cooled copper support. Depending on the pre-monochromator slit settings, one can achieve a wavelength (energy) bandpass $\Delta\lambda/\lambda$ ($\Delta E/E$) of $3–5 \times 10^{-4}$. The next element downstream is a toroidal mirror which is located at a distance of 17 m,

[1] Present address: Stanford Linear Accelerator Center, MS 99, PO Box 4349, Stanford, CA 94309, USA.

[2] Present address: UMIST, PO Box 88, Manchester, M60 1QD, UK.

half way between source and sample, providing a focal spot of approximately 4×0.4 mm^2 at the sample position. This mirror consists of eight gold-coated quartz segments pre-aligned on an optical bench, which can be positioned into the beam as a complete unit. Optimal focusing conditions are achieved with a beam incidence angle of 3.5 mrad, which results in a cut-off energy of approximately 20 keV, thus effectively suppressing the third harmonic radiation from the monochromator. The highest beam intensity is reached below the gold absorption edge (around the Se *K*-edge at a wavelength of 1 Å), although diffraction experiments down to 0.9 Å are carried out routinely and occasionally are also performed at wavelengths as short as 0.77 Å.

An energy stabilization device ensures that the X-ray energy remains constant during long-lasting critical experiments, *e.g.* the data collection at the inflection point or at the narrow white line of an absorption edge. This stabilizer originally developed for EXAFS spectroscopy (Pettifer & Hermes, 1985; Evans & Pettifer, 1996) consists of a perfect Si(220) crystal with a central hole which intercepts part of the X-ray beam before it travels on into the collimator and onto the sample. At specific energies, *i.e.* whenever the Bragg condition is fulfilled, X-rays are reflected back into two plastic scintillation detectors and registered. By changing the orientation of the Si crystal with respect to the incoming beam, these marker reflections can be detected at the precise wavelength of interest for the experiment. By monitoring the normalized intensity of these reflections occurring at the particular wavelengths, it is possible to trace minute wavelength drifts and change the monochromator angle to re-establish the correct wavelength. The accuracy of this device is of the order of 10^{-5}, *i.e.* one order of magnitude better than the bandpass of the monochromator.

In the experimental hutch all essential components, including the wavelength stabilizer, the collimator with intensity monitors, the ϕ-axis sample goniostat and the detector, are mounted on an optical bench, which is remotely aligned into the beam. Since all movements of the bench are about a virtual pivot point located in the center of the first collimator slits, intensity optimization is straightforward and well suited for automation. The collimator consists of two sets of adjustable slits separated by 200 mm defining the beam in both vertical and horizontal directions. Behind each pair of slits, integrated ionization chamber detectors monitor the intensity, allowing fast alignment of the collimator, optimization of the X-ray beam, as well as a normalization of exposure times for successive images of diffraction data.

Protein crystals are mounted on a ϕ-goniostat equipped with a video microscope whose cross-wire defines the intersection point of the X-ray beam and ϕ-rotation axis. A TV monitor inside the experimental hutch is used for crystal centering, whereas a monitor outside allows the observation of the sample's position and state during the experiment. The fluorescence of the protein sample is measured by a solid-state detector (XR-100T; Amptek Inc., Bradford, MA, USA) operated at room temperature providing – down to X-ray energies of around 6 keV – sufficient energy resolution to separate background and characteristic fluorescent radiation. This detector is mounted at right angles to the incoming beam direction and parallel to its polarization vector in order to reduce the high background from photons scattered elastically and inelastically by the sample. A multi-channel analyzer records the energy distribution of photons measured by the detector and only allows the counting of those photons corresponding to the fluorescence energy window for the correct atom for further processing. Thus absorption edges can be measured with high signal-to-noise ratio even from small samples, facilitating the proper choice of the energy positions for the subsequent diffraction experiments and good estimates for f' and f''. Typically, it is possible to measure an f'' of at least five electrons at the selenium *K*-edge white line.

All beamline components are controlled from a personal computer connected to a CAMAC crate, which hosts stepper motor controllers, rate-meters, scalers and other ancillary control equipment. The software routines that have been developed at the EMBL Hamburg Outstation control all motor movements and process the output of various beamline detectors. Specific programs can be run to perform complex tasks automatically, for example optimal alignment of the optical bench and collimator, fluorescence scans and wavelength stabilization, which runs continuously during data collection. Currently a Mar345 image-plate detector mounted on an extended translation stage is installed on the beamline. A maximum crystal detector distance of 675 mm can be reached with this configuration. The MarResearch software on a Unix workstation controls data collection including shutter control and ϕ-rotation. An Oxford Cryostream system for routine low-temperature data-collection completes the sample environment.

3. Overview of BW7A

Beamline BW7A is built on a multipole wiggler insertion device and receives about half of the available 3 mrad fan of radiation. The second half is directed towards the high-intensity fixed-wavelength beamline BW7B (van Silfhout & Hermes, 1994). The optical elements of beamline BW7A were specifically designed for MAD experiments in macromolecular crystallography. The fluorescence scan that precedes the data collection requires wavelength changes in small steps around the absorption edge of a given heavy atom. The beamline specifications can be summarized as follows: (i) point focusing of the beam at the sample position with a 3:1 demagnification; (ii) energy resolution of 1×10^{-4}; (iii) high scattering vector resolution ($< 2 \times 10^{-3}$ Å); energy range of 8–15 keV (0.7–1.8 Å); (iv) harmonic rejection better than 10^{-3}. These goals were achieved by implementing the design depicted in Fig. 1.

The first grazing-incidence water-cooled flat Rh-coated SiC mirror, which is located approximately 25 m from the source, absorbs most of the undesired high-energy synchrotron radiation produced by the wiggler. The second mirror is located downstream of the monochromator. This segmented quartz mirror is used for focusing and directing the synchrotron beam onto the sample. The combination of both mirrors set at a suitable glancing-incidence angle (3 mrad) rejects any higher-harmonic synchrotron radiation. The double-crystal monochromator features a directly water-cooled flat first crystal followed by a sagitally bent second crystal. Since the second crystal is placed at the center of the Bragg-angle rotation stage, a fixed-exit beam geometry is obtained. The second crystal is bent by a novel pneumatic actuator system, which allows a dynamic focusing of the monochromatic X-ray beam (Fig. 2). On this picture all degrees of rotational and translational movements are indicated as arrows. The possibility of fast energy changes is accomplished by placing both crystals on a disc that can be rotated by a single rotation stage (van Dijken & van Silfhout, 2000). The performance of the focusing monochromator system is shown in Fig. 3. The focal spot at the sample position is currently approximately 2.5 mm horizontally and 0.8 mm vertically, *i.e.* dictated by the relatively large source size and not by the optical system.

The collimator system, the single-axis ϕ-goniostat and the area detector are mounted on an optical table on kinematic mounts that allow a precise positioning with five degrees of freedom to optimize the intensity at the sample position (van Silfhout, 1998). The collimator system is similar to the one described for beamline X31.

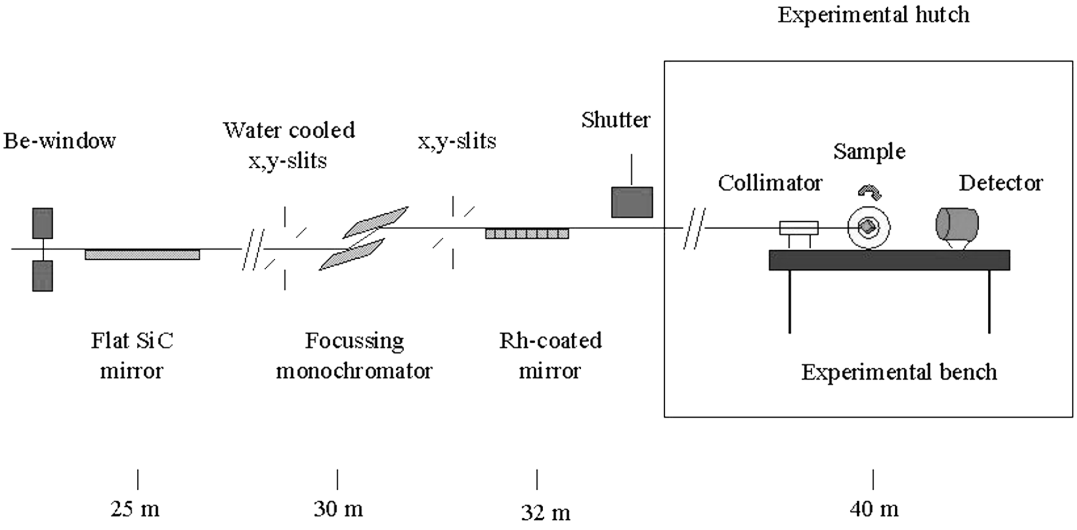

Figure 1
Schematic representation of beamline BW7A. The synchrotron radiation travels from left to right onto the sample.

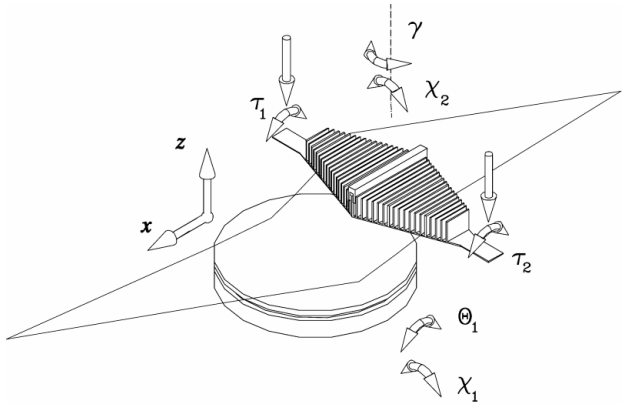

Figure 2
Design of the sagitally focusing double-crystal monochromator (van Dijken & van Silfhout, 2000). All possible rotational and translational movements are indicated with arrows. The motors are controlled *via* interactive *Labview* programs running on a personal computer.

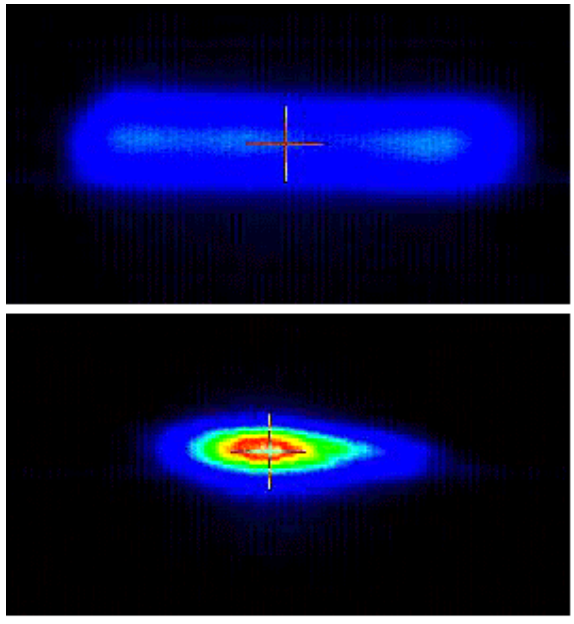

Figure 3
Profile of the unfocused (upper) and focused (lower) beam on BW7A. The horizontal width in the upper picture is defined by the slits. The image is color coded with highest intensity in white and lowest in blue. Please note that the focused beam was attenuated with the respect to the unfocused and therefore the displayed intensities are on a different scale. The size of each picture corresponds to 13×7 mm.

Two sets of slits that are 200 mm apart define the vertical and horizontal direction of the beam. The position of the beam on each side of the collimator is measured by quadrant photodiodes. The intensity is measured by ionization chambers behind each pair of slits. At a slit setting of 0.4×0.4 mm^2 the flux at a wavelength of 1 Å is approximately 8×10^{11} photon/sec which is approximately two orders of magnitude higher than the flux on beamline X31.

On beamline BW7A all components are controlled by interactive *Labview* programs developed in-house. These programs allow the automatic optimization of the table position with respect to the beam. In addition, the optimization of the curvature of the focusing monochromator crystal is performed semi-automatically using a screen that is turned into the beam. A video camera transfers the image of the focused beam to a personal computer and the position and the focus of the second monochromator crystal is then optimized interactively. The optical table is equipped with a crystallographic end-station developed in-house. This station consists of a ϕ-axis goniostat with integral angle encoder for crystal rotation, adjustable beam stop and a video microscope for crystal viewing and centering. Similar to the set-up at beamline X31, one TV monitor inside the hutch is used

for crystal centering whereas the second monitor outside displays the crystal during data collection. The Mar165 CCD area detector is mounted on a translation stage equipped with an absolute distance encoder. The minimum and maximum sample-to-detector distances are 35 mm and 1198 mm, respectively. Thus, with a given detector diameter of 165 mm the maximum resolution available is approximately 0.9 Å at the Se-edge energy. In addition, the detector can be lifted by a maximum of 8 cm in order to collect higher-resolution diffraction data at a given crystal–detector distance (Morris & Lamzin, 2001). The fluorescence scan of the crystal is performed using a similar solid-state detector as the one described for beamline X31 which allows energy-selective measurement. This scan is controlled by a graphical user interface (GUI) developed in collaboration with Daresbury Laboratory and Francis Goulding Associates. The interface is written in portable Java code and is running on a Silicon Graphics workstation. The program allows the user to simply choose the element of interest, perform the fluorescence scan and analyze the scan using the program *CHOOCH* which calculates f' and f'' from the experimental scan (Evans & Pettifer, 2001). The program communicates *via* TCP/IP protocols with the underlying *Labview* programs and the multi-channel analyzer software. An example of a fluorescence scan from an Se-Met containing protein crystal (dimensions $0.2 \times 0.2 \times 0.05$ mm) is displayed in Fig. 4.

The protein crystal mounted on the ϕ-goniostat for data collection can be cooled to cryogenic temperatures using an Oxford Cryostream system. The actual data collection is controlled by the MarResearch program running on a LINUX-based personal computer. This program also controls the local shutter and the exposure times. On both beamlines, data can be collected in time mode where each frame is exposed for the same time or in dose mode where the exposure time is calculated for each frame to achieve a preset exposure dose using the ionization chamber readings. The images are being stored on local disks and data processing can be performed on fast dual processor Compaq alpha server.

4. Performance during the last years

During 1999 the DORIS III storage ring provided synchrotron radiation from 25 January to 20 December with seven blocks of beam time interrupted by one week for maintenance after each block. Overall synchrotron radiation was made available for a combined period of about 35 weeks. In 2000 the ring was delivering synchrotron radiation from 6 January to 2 October in seven blocks of beam time for a total time period of approximately 33 weeks. Each year, approximately 20% of the beam time are allocated for internal research projects including the installation of technical upgrades, the testing of new equipment, and the collection of diffraction data for in-house projects.

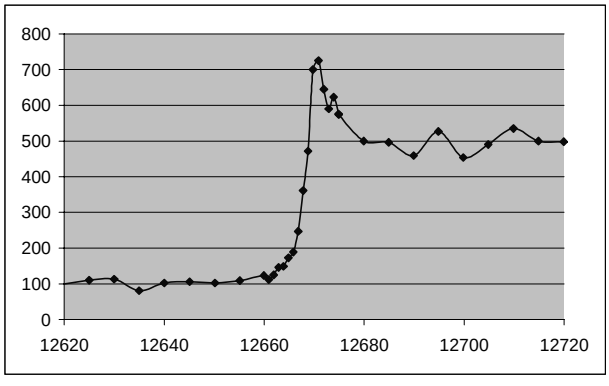

Figure 4
Fluorescence scan from a Se-Met substituted protein crystal. The crystal dimensions were approximately $0.2 \times 0.2 \times 0.05$ mm (Tucker & Mapelli, 2001). The fluorescence counts are given as a function of energy (eV).

4.1 *Performance of X31*

During 1999, 20 complete MAD experiments were performed on beamline X31. Each of these experiments was given between two and seven days of beam time with an average of approximately four days per MAD project (these numbers are calculated using our internal statistics and are based on the user logbook entries). It should be noted that this time includes the time required for the entire set-up for data collection (mounting of the samples, selection of a suitable crystal, fluorescence scan, set-up of the energy calibration and data collection at up to four wavelengths). For nine of the external projects we received user reports of a successful data collection later. During 2000, ten complete MAD experiments were performed with an average time of approximately four days of beam time per experiment. In addition, a number of projects received between half a day and three days of beam time (63 in 1999 and 56 in 2000). In many cases SAD data were collected from heavy-atom derivatives at the peak wavelength or slightly above in order to optimize the anomalous signal for SIRAS/MIRAS (single/multiple isomorphous replacement with anomalous scattering) phasing. Data collected at beamline X31 were also successfully used for collecting atomic resolution data (<1.1 Å) of large small-molecules for *ab initio* structure solution using direct methods (Gessler *et al.*, 1999). Examples for successful MAD structure solution using data collected in the last years include the structures of the human β2 glycoprotein 1 (Schwarzenbacher *et al.*, 1999), the DNA Holiday junction (Ortiz-Lombardia *et al.*, 1999), the Saccharopine reductase from *M. grisea* (Johansson *et al.*, 2000) and the ligand binding domain of axonin/TAG1 (Freigang *et al.*, 2000). The bacterial D-hydantionase from *Thermus sp.* represented the largest structure solved using MAD data collected on beamline X31 (Abendroth *et al.*, 1999). The enzyme consists of 458 residues and includes nine selenomethionines per monomer. The protein crystallized in space group $C222_1$ with unit cell dimensions of a = 125.1 Å, b = 215.2 Å and c = 207.6 Å. There are six copies per asymmetric unit thus containing 54 selenium atoms. Complete diffraction data to a resolution of 2.5 Å were collected at three energies at 0.9184 Å (high-energy remote), 0.9794 Å (inflection point) and 0.9797 Å (peak) over a period of seven days. It is important to note that the automatic wavelength calibration described above is essential to ensure a constant wavelength over this long period of time. All 54 Se sites were located using the automatic procedure implemented in *SOLVE* (Abendroth *et al.*, 2000).

4.2 *Performance of BW7A*

Starting from July 1999 the wiggler beamline BW7A has been used routinely by the structural biology community. During the second half of the year, 25 complete MAD experiments were performed with an average of approximately three days of beam time for each MAD experiment. In ten cases we received reports describing the data collection. In 2000, 40 MAD experiments were performed with an average beam time of two days. The shorter time per experiment is due to the higher intensity of the wiggler and the fast read-out of the CCD detector. In addition to these MAD experiments, beam time on BW7A was given to 39 and 46 projects in 1999 and 2000, respectively. Many of these projects also included SAD data collection at the optimized

Table 1
Selected MAD projects solved by groups of the EMBL Hamburg Outstation during the last two years.

	HisA (*a*)	HisF (*a*)	GAPN (*b*)	TrpD (*c*)	POU-DNA (*d*)	DNA-Holliday junction (*e*)
Molecular weight [kDa]	27.0	27.7	55	37	50	12.5
Molecules per asym. unit	2	1	1	4	1	1
Crystal dimensions [mm]	$0.3 \times 0.1 \times 0.1$	$0.3 \times 0.2 \times 0.2$	$0.3 \times 0.3 \times 0.5$	$0.2 \times 0.15 \times 0.05$	$0.7 \times 0.5 \times 0.4$	$0.3 \times 0.3 \times 0.05$
Cell dimensions a,b,c [Å]	46.4, 72.9, 62.0	79.6, 44.4, 63.9	185.2, 185.2,132	92.3, 65.8, 114.5	131.2,131.2,117	23.8, 63.9, 71.4
α,β,γ [°]	90, 98.9, 90	90, 112, 90	90, 90, 120	90, 107.5 90	90, 90, 120	90, 90, 90
Space group	$P2_1$	C2	$P6_222$	P2	$P6_222$	$C222_1$
Beamline	BW7A	BW7A	BW7A	BW7A	BW7A	X31
Detector	Mar300	Mar300	Mar300	Mar300	MarCCD	Mar 180 mm
Detector type	Imaging plate	Imaging plate	Imaging plate	Imaging plate	CCD	Imaging plate
Temperature [K]	100	100	100	100	100	100
Resolution [Å]	2.34	1.85	2.9	2.9	2.85	2.7
Anomalous Scatterer	Se	Se	Se	Se	Br	Br
No. of wavelengths	3	3	3	3	3	4
Wavelength peak	0.9787	0.9789	0.9792	0.9797	0.9185	0.9220
Wavelength inflection	0.9791	0.9796	0.9796	0.9800	0.9190	0.9224
Wavelangth remote	0.9807	0.9808	0.9724	0.9000	0.8856	0.8856 and 1.250
ϕ-range (infl./peak/remote)	309, 319.5, 309.5	258, 285.6, 232.2	60.5, 58, 41.5	180, 360, 180	98,174,96	90
ϕ per frame	1.5	1.2	0.5	1.0	1.0	1.0
Appr. time/frame [min]	1–2	1–2	5–7	6–8	4–5	6–8
Data collection time [h] #	48	48	48	80	24	42
Structure solution/phasing	SHARP/SOLVE	SHARP/SOLVE	SOLVE	RSPS/SHARP	SHELX/SHARP	MLPHARE
No. of sites per asu	6	6	9	28	4	4
No. of sites used in phasing	3	5	8	26	4	4

(*a*) Lang *et al.* (2000); (*b*) Pohl *et al.* (2001), (*c*) Mayans & Wilmanns (2001), (*d*) Remenyi *et al.* (2001), (*e*) Ortiz-Lombardia *et al.* (1999).
(*c*) The data were collected under low-bunch conditions which reduces the photon flux by approximately a factor of two.
Data-collection time including preparation of the experiment, selection of a suitable crystal, crystal mounting and fluorescence scans.
* These 26 sites were found by a combination of RSPS (Knight, 2000), interpretation of various Patterson functions and difference Fourier analysis. Details will be published elsewhere (Mayans & Wilmanns, 2001).

anomalous signal of heavy-atom derivatives for SIRAS/MIRAS phasing. Other projects made particular use of the availability of shorter wavelengths. One example is the data collection performed at 0.54 Å resolution for Crambin to calculate valence electron distribution in a small protein (Jelsch *et al*., 2000). Examples of successful structure solutions using MAD data collected on beamline BW7A include the human release factor eRF1 (Song *et al*., 2000), the complex of the ribosomal protein S15 with rRNA (Nikulin *et al*., 2000), the structure of the 5′-nucleotidase from *E. coli* (Knöfel & Sträter, 1999) and the ATPase subunit of the tetrahalose/maltose transport (Diederichs *et al*., 2000).

4.3 *In-house MAD projects during 1999/2000*

A number of crystal structures have been solved using MAD data collected in-house by research groups of the EMBL Hamburg Outstation (alone or in collaboration with external groups). The six examples given here can be used to illustrate the requirements for successful phase determination using data collected on our tunable protein crystallography beamlines. Data-collection parameters are summarized in Table 1. The crystal dimensions range from 50 µm to 0.5 mm and the unit-cell sizes vary from 24 to 185 Å. The maximum resolution limits range from 1.85 to 2.9 Å, which is fairly typical for all MAD data sets collected on these beamlines. Four out of the six structures contained Se-Met substituted protein whereas the remaining two cases included brominated DNA-oligonucleotides. In five cases the structure solution and phase determination was straightforward, and in four out of the six examples most heavy-atom sites were found automatically by different programs. In these cases interpretable maps were calculated within a few days of experiment completion. In the case of TrpD the structure solution was hindered by pseudo-symmetry caused by special non-crystallographic symmetry. The heavy-atom positions were finally found by a combination of Patterson and Fourier methods (Mayans & Wilmanns, 2001).

The crystal structure determination of the non-phosphorylating glyceraldehyde-3-phosphate dehydrogenase (GAPN) from the hyperthermophilic Archaeum *Thermoproteus tenax* represents a typical example for a MAD data collection (Fig. 5*a*). This structure exemplifies the quality of experimental electron density maps that can be obtained at modest resolution. Details of the crystal structure analysis are given elsewhere (Pohl *et al*., 2001). The protein crystallizes in space group $P6_222$ with unit cell dimensions of $a = b =$ 185 Å, and $c = 132$ Å (Brunner *et al*., 2000). The Se-Met substituted protein crystals diffracted to 2.9 Å only. A three-wavelength MAD experiment was performed on the EMBL wiggler beamline BW7A using a Mar300 imaging-plate detector (further experimental details are given in Table 2). After data processing using *DENZO* and *Scalepack* (Otwinowski & Minor, 1997), eight out of nine heavy-atom positions were automatically identified with the programs *SOLVE* (Terwilliger & Berendzen, 1999) and *SHELXD* (Sheldrick, 1998). Heavy-atom refinement and phase calculations were subsequently performed with *SOLVE* resulting in a figure-of-merit of 0.57. Solvent flattening and histogram matching using *DM* (Cowtan, 1999) increased the figure-of-merit to 0.76. The resulting electron density map depicted

Table 2
Summary of MAD data collection of Se-Met GAPN crystals (Pohl *et al*., 2001).

Data type	Inflection	Peak	Remote
Wavelength [Å]	0.9796	0.9792	0.9724
Resolution [Å]	30-2.9	30-2.9	30-2.9
No. measurements	435028	449891	311073
No. unique	30087	30141	30085
Completeness [%]			
Overall	99.6	98.7	96.5
Last shell	100	100	99.4
R_{merge}*			
Overall	0.061	0.070	0.055
Last shell	0.57	0.42	0.57
Average I/σ(I)			
Overall	27.0	19.7	22.2
Last shell	5.0	7.0	4.0

* R_{merge} = SUM [(Abs(I – ⟨I⟩)]/SUM(I).

Table 3
Number of MAD experiments with the anomalous scatterer performed on beamlines X31 and BW7A in 1999 and 2000.

	1999	1999	2000	2000
Element	X31	BW7A	X31	BW7A
Fe	1	1	1	4
Cu	-	-	-	1
Zn	-	1	-	2
As	-	-	1	1
Se	8	15	3	17
Br	3	1	1	2
Sm	-	-	-	1
Eu	1	-	-	-
Yb	1	-	-	1
Ta	1	-	-	-
Re	-	1	-	-
Os	1	-	-	-
Ir	-	-	-	1
Pt	2	2	2	2
Au	-	-	-	1
Hg	2	3	2	6
U	-	1	-	1
Total	20	25	10	40

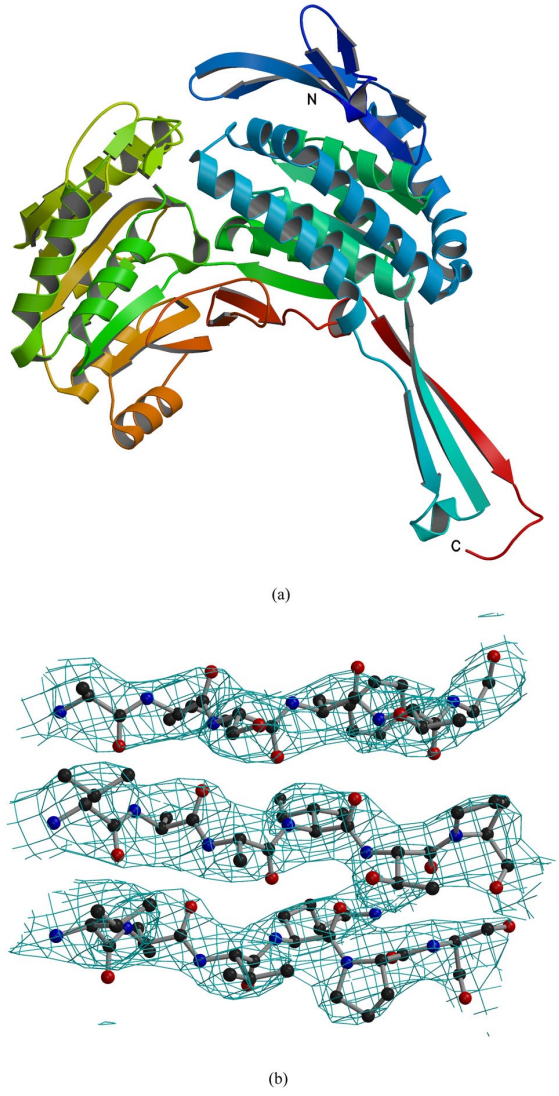

Figure 5
(a) Ribbon diagram of the non-phosporylating glyceraldehyde-3-phosphate dehydrogenase (GAPN) from *T. tenax* solved by MAD analysis (Pohl *et al*., 2001). The colour is changing from the N-terminus in blue to the C-terminus in red. This figure was produced using *Molscript* (Kraulis, 1991) and *raster3D* (Merritt & Beacon, 1997). (b) Electron density of a typical section of the protein using the experimental phases based on eight selenium atoms after solvent flattening and histogram matching with data from 30 to 2.9 Å. The current crystallographic model is superimposed. This figure was generated using *Bobscript* (Esnouf, 1997).

In Fig. 5(*b*) was clearly interpretable and the model could almost be completely built using the interactive graphical program *O* (Jones *et al*., 1991).

4.4 *Statistics of all MAD projects in 1999/2000*

The summary of all MAD data sets collected on both beamlines and including the anomalous scatterer is shown in Table 3. In 1999, 45 MAD experiments were collected on X31 and BW7A. The number of MAD data sets increased to 50 in 2000. This increase was mainly due to the improvements on the wiggler beamline described above. They decreased the average time per project allowing more projects to receive beam time on BW7A. Thus, the higher throughput on BW7A allowed that beamline X31 was used to search for heavy-atom derivatives while the MAD data collection was performed on the higher-intensity beamline BW7A. This might explain the decreasing number of complete MAD data sets collected on X31. The analysis of the anomalous scatterers used shows that the most common element in MAD experiments was Se in selenomethionine substituted protein crystals (23 out of 45 in 1999, and 20 out of 50 in 2000). Our results illustrate the growing importance of recombinant protein expression. The second most frequently used element is mercury (five in 1999, and eight in 2000), usually in the form of heavy-atom derivatives with platinum and bromine in third and fourth place. In addition, an increasing variety of heavy-atom derivatives ranging from samarium to uranium have been successfully used.

5. Conclusion and future plans

Over the last years the two tunable EMBL beamlines suitable for the collection of multiple anomalous diffraction data have been constantly upgraded and improved. High-quality SAD and MAD data sets can

now be collected routinely on both beamlines and due to the advances in computing structures are now often being solved before the data collection is finished. Whereas the typical time for a full experiment including sample preparation on X31 requires up to four days, the time has decreased to about two days on the wiggler beamline BW7A. We anticipate that the time will be further reduced in the near future. The statistics of all projects shows that although a high proportion of successful MAD experiments were performed at the selenium edge using recombinant Se-Met substituted protein crystals, the majority of projects utilized various other heavy atoms. These are, for example, metalloproteins, proteins or biological complexes that are purified from the natural source or DNA-binding proteins. Our summary clearly demonstrates the need for a wide range of accessible energies and the necessity for fast and reliable energy changes.

Our future plans can be divided into three sections: (i) improvement of the optical elements to increase the intensity; (ii) improvements of the crystallographic end-stations in order to increase the user-friendliness and decrease the time required to set up the experiment; (iii) further automation of data collection and structure solution. The bending magnet beamline X31 is inherently significantly weaker than the wiggler beamline BW7A. In addition, most optical elements of X31 have been in continuous operation for more than ten years. Thus, it is planned to concentrate on the intensity improvement by gradually replacing the optical elements so that the beamline remains operational for most of the scheduled beam time. The first improvement would be to replace the second gold-coated segmented mirror by a continuous Rh-coated focusing mirror. We estimate that this new mirror would lead to an increase in X-ray intensity at the sample position by at least a factor of two.

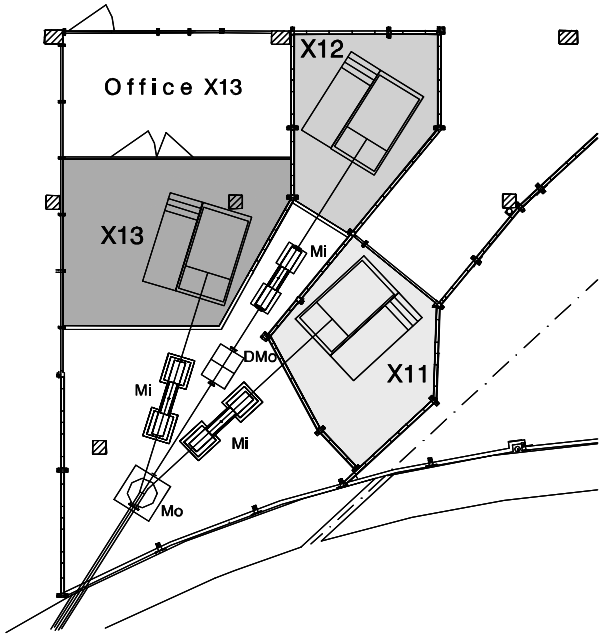

Figure 6
Ground floor plan of the ongoing reconstruction of the EMBL beamlines on fan K of DORIS III. The central beamline X12 will be used for MAD experiments, the flanking beamlines X11 and X13 are operated at fixed wavelengths. Mo: triangular, horizontally focusing monochromator; Mi: vertically focusing rhodium-coated mirror; DMo: sagitally focusing double-crystal monochromator.

The prospective plans for the wiggler beamline BW7A are primarily centered on improving the optical system and the interactive user control. Currently, the SiC mirror closest to the source is flat and hence the monochromator cannot accept the full vertical divergence. Replacing this optical element by a parabolic mirror would increase the available flux by a factor of two. In addition, the segmented focusing mirror can be replaced by a continuous mirror, bent into ellipsoidal shape by two bending moments and located closer to the sample. This set-up would further increase the available flux density at the sample. Since the data-collection time has considerably decreased due to improvements of the optical elements, the time required to set up the experiment should decrease too. Therefore it is planned to further automate the initial steps of data collection including the fluorescence scan thus minimizing the access to the experimental hutch. The next step of automation encompasses the crystal mounting and centering. For automatic centering it is necessary to motorize the *x*,*y*,*z*-movement of the crystal and to transfer the image taken by the video microscope to a personal computer where the center of the crystal is determined by special image-recognition software currently under development. Subsequently, the crystal mounting of pre-cooled crystals will be automated and remotely controlled. Automatic mounting systems have already been developed, or are under development, by several groups including Abott Laboratories (Muchmore *et al.*, 2000) and the EMBL/ESRF (Perrakis, Cipriani *et al.*, 1999). We are planning to develop an automatic system along similar lines.

All these improvements will be implemented on the two wiggler beamlines BW7A and BW7B first, and after sufficient testing will be used on other EMBL beamlines. The increasing automation of synchrotron beamlines is of particular importance considering the current and future structural genomics projects worldwide (see the recent supplement *of Nature Structural Biology*, published in November 2000). It is clear that the demand for beam time on tunable sources will continue to exceed the available time on the existing facilities. We therefore recently started the reconstruction of X11, X12 and X13, the three EMBL bending-magnet beamlines sharing radiation from fan K of DORIS III. The former optics and test station X12 will be replaced by a tunable protein crystallography beamline complementing the flanking fixed-wavelength stations X11 and X13. Fig. 6 shows a floor plan of the three stations schematically indicating the positions of various optical elements. The first optical elements are the monochromator crystals (designated Mo in Fig. 6) that take approximately one-third on each side of the fan and direct the radiation to the fixed-wavelength beamlines X11 and X13, respectively. The remaining central part will be used for the tunable beamline X12. In adopting for X12 a similar design as BW7A, we hope to minimize the time until the first experiments can be performed. The key component of this beamline will be a sagitally focusing fixed-exit Si (111) double-crystal monochromator (DMo in Fig. 6) similar to the design implemented on beamline BW7A. This monochromator system ensures stability and fast uncomplicated wavelength changes. The anticipated heat load is considerably lower compared with the wiggler beamlines where this constituted the main source of problems. Despite the relaxed thermal situation for the monochromator we intend to install a wavelength stabilization device to achieve the maximum anomalous signal during longer experimental runs. In order to compensate for the significantly lower brightness of this bending-magnet beamline we are planning to introduce a new high-quality continuous mirror with improved focusing properties. The first continuous mirror of this kind has recently been tested on beamline X13 and resulted in a three-fold increase in intensity compared with the segmented mirror (Hermes, 2000). The experimental hutch will house a similar crystallographic

end-station equipped with the automated system we are currently developing for other beamlines. We anticipate that the construction of the new MAD beamline X12 will be finished by the beginning of 2002.

The design, construction and maintenance of the beamlines are only possible with the work of many people. We would like to thank Thomas Gehrmann, Victor Renkwitz, Roy Kläring and Bernd Robrahn for their contributions. We are grateful to Drs Jan Abendroth, Dietmar Schomburg (University of Cologne), Olga Mayans and Marina Mapelli (EMBL Hamburg Outstation) for communicating their results prior to publications, and we thank Drs Matthias Wilmanns, Paul Tucker and Victor Lamzin for their ongoing support and many valuable discussions.

References

Abendroth, J., Niefind, K. & Schomburg, D. (1999). HASYLAB/EMBL: Annual User Report 1999. p. 139. HASYLAB, Hamburg, Germany.
Abendroth, J., Niefind, K., Chatterjee, S. & Schomburg, D. (2000). *Acta Cryst*. D**56**, 1166–1169.
Amemiya, Y. (1997). *Methods Enzymol*. **276**, 233–243.
Brünger, A. T., Adams, P. D., Clore, G. M., DeLano, W. L., Gros, P., Grosse-Kunstleve, R. W., Jiang, J.-S., Kuszewski, J., Nilges, M., Pannu, N. S., Read, R. J., Rice, L. M., Simonson, T. & Warren, G. L. (1998). *Acta Cryst*. D**54**, 905–921.
Brunner, N. A., Lang, D. A., Wilmanns, M. & Hensel, R. (2000). *Acta Cryst*. D**56**, 89–91.
Cassetta, A., Deacon, A. M., Ealick, S. E., Helliwell, J. R. & Thompson, A. W. (1999). *J. Synchrotron Rad*. **6**, 822–833.
Cowtan, K. (1999). *Acta Cryst*. D**55**, 1555–1567.
Dauter, Z. & Dauter, M. (1999). *J. Mol. Biol.* **289**, 93–101.
Dauter, Z., Dauter, M., Fortelle, E., Bricogne, G. & Sheldrick, G. M. (1999). *J. Mol. Biol.* **289**, 83–92.
Diederichs, K., Diez, J., Greller, G., Müller, C., Breed, J., Schnell, C., Vonrhein, C., Boos, W. & Welte, W. (2000). *EMBO J.* **22**, 5952–5961.
Dijken, S. van & Silfhout, R. G. van (2000). *AIP Conf. Proc.* **215**, 304–307.
Doublie, S. (1997). *Methods Enzymol*. **276**, 523–530.
Esnouf, R. M. (1997). *J. Mol. Graph*. **15**, 133–138.
Evans, G. & Pettifer, R. F. (1996). *Rev. Sci. Instrum*. **67**, 3428–3433.
Evans, G. & Pettifer, R. F. (2001). *J. Appl. Cryst.* **34**, 82–86.
Fourme, R., Shepard, W., Schiltz, M., Prangé, T., Ramin, M., Kahn, R., de la Fortelle, E. & Bricogne, G. (1999). *J. Synchrotron Rad*. **6**, 834–844.
Freigang, J., Proba, K., Leder, L., Diederichs, K., Sonderegger, P. & Welte, W. (2000). *Cell*, **101**, 425–433.
Garman, E. F. (1999). *Acta Cryst*. D**55**, 1641–1653.
Garman, E. F. & Schneider, T. R. (1997). *J. Appl. Cryst.* **30**, 211–237.
Gessler, K., Uson, I., Takaha, T., Krauss, N., Smith, S. M., Okada, S., Sheldrick, G. M. & Saenger, W. (1999). *Proc. Natl. Acad. Sci. USA*, **96**, 4246–4251.
Grosse-Kunstleve, R. W. & Brünger, A. T. (1999). *Acta Cryst.* D**55**, 1568–1577.
Helliwell J. R. (1992). *Macromolecular Crystallography with Synchrotron Radiation*. Cambridge University Press.
Hendrickson, W. A. (1990). *Science*, **254**, 51–58.
Hendrickson, W. A. (1999). *J. Synchrotron Rad*. **6**, 845–851.
Hendrickson, W. A. & Teeter, M. M. (1981). *Nature*, **290**, 107–113.
Hermes, C. (2000). EMBL Annual Report 2000. EMBL, Hamburg, Germany.
Hope, H. (1988). *Acta Cryst*. B**44**, 22–26.
Jelsch C., Teeter, M. M., Lamzin, V., Pichon-Pesme, V., Blessing, R. H. & Lecomte, C. (2000). *Proc. Natl. Acad. Sci. USA*, **97**, 3171–3176.
Johansson, E., Steffens, J. J., Lindqvist, Y. & Schneider, G. (2000). *Structure*, **8**, 1037–1047.
Jones, T. A., Zou, J. Y., Cowan, S. W. & Kjeldgaard, M. (1991). *Acta Cryst.* A**47**, 110–119.
Knight, S. D. (2000). *Acta Cryst.* D**52**, 42–47.
Knöfel, T. & Sträter, N. (1999). *Nature Struct. Biol*. **6**, 448–453.
Kraulis, P. (1991). *J. Appl. Cryst*. **24**, 946–950.
La Fortelle, E. & Bricogne, G. (1997). *Methods Enzymol*. **276**, 472–494.
Lang, D., Thoma, R., Henn-Sax, M., Sterner, R. & Wilmanns, M. (2000). *Science*, **289**, 1546–1550.
Mayans, O. & Wilmanns, M. (2001). Unpublished results.
Merritt, E. A. & Beacon, D. J. (1997). *Methods Enzymol.* **277**, 505–525.
Morris, R. J. & Lamzin, V. L. (2001). In preparation.
Muchmore, S. W., Olson, J., Jones, R., Pan, J., Blum, M., Greer, J., Merrick, S. M., Magdalinos, P. & Nienaber, V. L. (2000). *Structure*, **8**, R243–R245.
Nikulin, A., Serganov, A., Ennifar, E., Tishchenko, S., Nevskaya, N., Shepard, W., Portier, C., Garber, M., Ehresmann, B., Ehresmann, C., Nikonov, S. & Dumas, P. (2000). *Nature Struct. Biol.* **4**, 273–277.
Ortiz-Lombardia, M., Gonzalez, A., Eritja, R., Aymami, J., Azorin, F. & Coll, M. (1999). *Nature Struct. Biol.* **6**, 913–917.
Otwinowski, Z. & Minor, W. (1997). *Methods Enzymol*. **276**, 307–326.
Perrakis, A., Cipriani, F., Castagna, J.-C., Claustre, L., Burghammer, M., Riekel, C. & Cusack, S. (1999). *Acta Cryst.* D**55**, 1765–1770.
Perrakis, A., Morris, R. & Lamzin, V. S. (1999). *Nature Struct. Biol.* **5**, 458–463.
Pettifer, R. F. & Hermes, C. (1985). *J. Appl. Cryst*. **18**, 404–412.
Phillips, W. C., Stanton, M., Stewart, A., Qian, H., Ingersoll, C. & Sweet R. M. (2000). *J. Appl. Cryst*. **33**, 243–251.
Pohl, E., Brunner, N. A., Wilmanns, M. & Hensel, R. (2001). In preparation for publication.
Remenyi, A., Tomilin, A., Pohl, E., Scholer, H. & Wilmanns, M. (2001). In preparation for publication.
Rice, L. M., Earnest, T. N. & Brünger, A. T. (2000). *Acta Cryst.* D**56**, 1413–1420.
Rodgers, D. (1997). *Methods Enzymol*. **276**, 183–203.
Schwarzenbacher, R., Zeth, K., Diederichs, K., Gries, A., Kostner, G. M., Laggner, P. & Prassl, R. (1999). *EMBO J.* **18**, 6228–6239.
Sheldrick, G. M. (1998). *SHELX: Application to Macromolecules*. *In Direct Methods for Solving Macromolecular Structures*, edited by S. Fortier, pp. 401–411. Dordrecht: Kluwer.
Silfhout, R. G. van (1998). *Nucl. Instrum. Methods Phys. Res. A*, **403**, 153–160.
Silfhout, R.G. van & Hermes, C. (1994). *Rev. Sci. Instrum*. **66**, 1818.
Smith, J. L. (1991). *Curr. Opin. Struct. Biol.* **1**, 1002–1011.
Song, H., Mugnier, P., Das, A. K., Webb, H. M., Evans, D. R., Tuite, M. F., Hemmings, B. A. & Barford, D. (2000). *Cell*, **100**, 311–321.
Tate, M. W., Eikenberry, E. F., Barna, S. L., Wall, M. E., Lowrance, J. L. & Gruner, S. M. (1995). *J. Appl. Cryst*. **28**, 196–205.
Terwilliger, T. C. & Berendzen, J. (1999). *Acta Cryst*. D**55**, 849–861.
Tucker, P. A. & Mapelli, M. (2001). Unpublished results.
Walsh, M. A., Dementieva, I., Evans, G., Sanishvilki, R. & Joachimiak, A. (1999). *Acta Cryst.* D**55**, 1168–1173.
Wilson, K. S. (1989). *Synchrotron Radiation in Structural Biology*, edited by R. M. Sweet & A. D. Woodhead. New York: Plenum.